THE ORIGIN OF THE PSEUDOGAP

YUVAL LUBASHEVSKY

THE ORIGIN OF THE PSEUDOGAP

RESEARCH THESIS

SUBMITTED IN PARTIAL FULFILLMENT OF THE

REQUIREMENTS

FOR THE DEGREE OF MASTER OF SCIENCE

IN PHYSICS

YUVAL LUBASHEVSKY

SUBMITTED TO THE SENATE OF THE TECHNION — ISRAEL INSTITUTE OF TECHNOLOGY

NISAN, 5767 HAIFA APRIL, 2007

THIS RESEARCH THESIS WAS SUPERVISED BY PROF. AMIT KEREN
UNDER THE AUSPICES OF THE PHYSICS DEPARTMENT

ACKNOWLEDGMENT

I would like to thank Prof. Amit Keren for the guidance, support and patient.

Special thanks to Rinat Ofer for her help at the beginning of this work.

THE GENEROUS FINANCIAL HELP OF THE TECHNION AND THE ISRAEL SCIENCE FOUNDATION IS GRATEFULLY ACKNOWLEDGED

Contents

List of Figures

Abstract

In this work we deduced the HTSC's Pseudogap critical temperature, known as $T^{\star}$. We did that by measuring the magnetic susceptibility on high temperatures region. We measured the CLBLCO system, in which small changes in the superconductivity properties can be made by making small changes in the chemical components. Changes of $T^{\star}$ can be detected as a function of the changes in the chemical components and ,of-course, as the function of the doping levels.

Previous work in our group demonstrated that in the cuprates superconductors: $T_c \propto J_f n_s$ where T_c is the superconductor transition temperature, J_f a magnetic energy scale for a given cuprates family, and n_s is the superconducting carrier density. We have also found correlation, using a scalling relation, between T_c^{max} (SC temperature at optimal doping), T_N (the Néel temperature) and T_g (the spin-glass temperature) for a given family.

in this work, we enhance this previous results by including $T^{\star}$ in the scaling relation. In addition, we found new properties of $T^{\star}$ by comparing it to the other critical temperature.

List of Symbols

HTSC	High Temperature SuperConductor
T_c	Superconductive critical temperature
T_N	Nèel antiferromagnetism critical temperature
T_g	Spin glass critical temperature
$T^\star$	Pseudogap critical temperature
n_s	Superfluid density
J	Energy scale
p	Doping level
T_c^{max}	T_c at the optimal doping point
T_N^{max}	T_N at the most underdoped point
x	Calcium level in CLBLCO
y	Oxygen level
y_0	Oxygen level at the optimal doping point
Δy	Oxygen level as measured from optimal doping
SQUID	Superconducting QUantum Interference Device
χ	Measured Susceptibility
χ_0	Real susceptibility

Chapter 1

Preface

The cuprates high T_c superconductors are ceramic compounds all having CuO_2 planes. These compounds are antiferomagnetic Mott insulators in their undoped state. Upon holes or electrons doping by chemical substitution or oxygenation at out-of-plane sites they become High T_c superconductors [HTSC] and the long range antiferromagnetism is destroyed. The origin of the magnetism at low doping levels lies in the CuO_2 planes, and superconductivity also occurs in these planes. In the undoped region the antiferomagnetic transition temperature (T_N) deceases with the doping level until it reaches zero at about 4% doping, where ordered antiferromagnetic state no longer exists. Above a certain doping level superconductivity emerges. The superconducting transition temperature (T_c) increases with doping, up to a point of "optimal doping" (T_c^{max}). After this point further doping results in a T_c reduction. In the region between long range antiferromagnetic order and the region with no magnetic moments, there is a random arrangement of frozen moments. This phase, called spin glass, exist in these compounds also in the underdoped superconducting state.

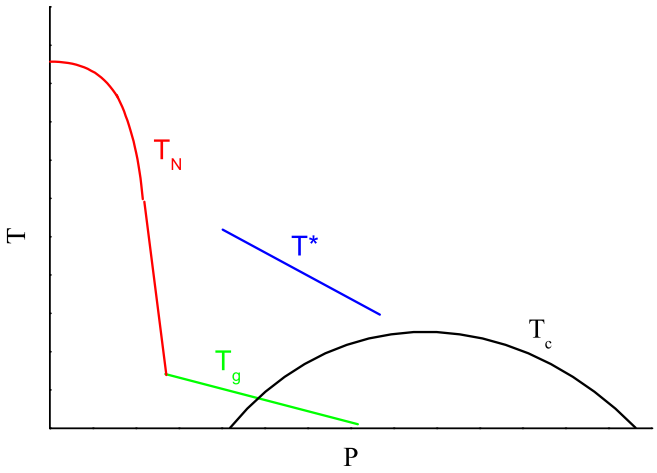

Figure 1.1: The cuperate phase diagram.

As a result of the intimate relation between the superconducting state and the antiferromagnetism, it is believed that superconductivity in the cuprates emerges from magnetic fluctuations in the same sense that BCS type superconductivity stems from lattice fluctuations (phonons). Moreover, unlike BCS superconductivity, in which the superconductivity energy gap opens together with the appearance of the superconducting phase (at T_c), in HTSC it has been noticed,in the underdoped region, that a kind of energy gap (Pseudogap) emerges at a temperature ($T^\star$) much higher than T_c. $T^\star$ decreases, approximately linearly, as the function of the doping, untill $T^\star$ and T_c merge at optimal doping. This phase diagram is shown qualitatively in Fig.
1.1. In this work I investigate the origin of the pseudogap by studying how $T^\star$ behaves as the function magnetic properties, where small changes in the chemical composition are an implicit parameter. In particular I am interested in the influence of the in-plane Heisenberg coupling constant (J_f) and out-of-plane ($J_f\alpha$) on $T^\star$. The variations in J_f and α are achieved by studying four different families of the

$(Ca_xLa_{1-x})(Ba_{1.75-x}La_{0.25+x})Cu_3O_y$ (CLBLCO) system, each having it own magnetic properties and superconducting dome but negligible structural changes. A review of this compound is given is section 2.1. The determination of $T^\star$ is done with susceptibility χ measurements as described in sections 3.7 and 5. Extraction of $T^\star$ from χ is discussed in sections 5 and 6. Finally, discussion and summary are given in sections 7 and 8.

The major finding of this work is that $T^\star$ dependes on J_f and α in the same way that T_N does. In other words, $T^\star \propto T_N$ and not just to J_f. This work enhances our group's previous experimental demonstration of simple relation between magnetic energy scale, doping, and T_c, by adding the $T^\star$ measurements. These results leave very little doubt that cuprate's superconductivity is a result of magnetic fluctuations.

Chapter 2

Materials

2.1 Structure and properties

$(Ca_xLa_{1-x})(Ba_{1.75-x}La_{0.25-x})Cu_3O_y$ (CLBLCO) is a unique family of HTSC in which one can vary the superconducting and magnetic properties with minimal structural changes. Therefore, it allows one to try and understand what are the physical rather than chemical properties of the material that govern superconductivity. CLBLCO belongs to the 1:2:3 system (atomic ratio). It's unit cell is very similar to the famous $YBa_2Cu_3O_y$ (YBCO), apart from the Ca which occupies the Y site, and the La which occupies both the Y and the Ba site. This compound is tetragonal in all it's range of existence $0 \leq x \leq 0.5$, so there are no ordered Cu-O chains like in YBCO; the oxygen atoms in the chain layer are distributed randomly with respect to the $\vec{a}$ and the $\vec{b}$ directions. According to bond valence sum calculation, the hole concentration in the CuO_2 planes does not depend on x, nevertheless, the maximum value of T_c varies from ~ 45 K at $x = 0$ to ~ 80 K at $x = 0.4$ [1].

The CLBLCO family is stable over a wide range of doping so one can synthesize

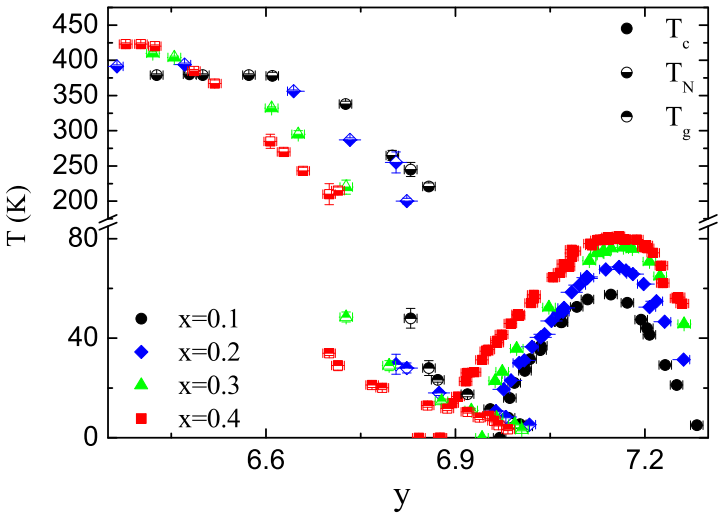

Figure 2.1: CLBLCO phase diagram.

samples ranging from the parent antiferromagnetic compound, to underdoped superconductors, and even to the overdoped superconductors, by changing the oxygen content. In addition, by changing x, very similar T_c and T_N versus oxygen doping curves are formed, as shown in the phase diagram, figure 2.1. In the doping region up to $y \sim 6.5$, the T_N curves of the different families are nearly parallel, where the $x = 0.1$ family have the lowest value of T_N, and the $x = 0.4$ is the highest. In the superconductivity regime, $y \sim 6.9$ to $y \sim 7.25$, the families are still behaving in a parallel order, with a shift between them, and the T_c of the $x = 0.4$ family is still the highest one. On the boundary region, where we can not identify a Néel order any more, and the superconductivity phenomena haven't emerge yet, it is possible to measure the T_g, which is the "freezing" temperature, in which domains of spin becomes spin-glass. T_g behave very similar to the T_N.

Chapter 3

Theoretical review

The magnetic susceptibility χ_0 is defined as the ratio between the magnetization and H_{in}^{total}, the total inner-sample field. For small enough applied magnetic fields the magnetization will be a linear function of this field.

We work out the case where a sphere is not magnetized on its own, but the applied current, and therefore field H, is causing it to be magnetized. We further assume that as a result of the external field the material is magnetized in the same direction as the external field. The magnetization M is proportional to the current in the surface of the sphere. Therefore,

$$H_{in}^{total} = H - DM$$

Where D is known as the magnetizing factor, and it has different values for different geometries.

$$M = \chi_0 H_{in}^{total} = \chi_0 (H - DM)$$

so that

$$M = \frac{\chi_0}{1 + D\chi_0} H$$

where $D = \frac{4\pi}{3}$ for a sphere. We define the measured susceptibility χ_{dc} by

$$\chi_{dc} = \frac{\chi_0}{1 + D\chi_0}.$$

For a needle like sample $D = 0$. We are interested in χ_0, which is obtained using a cylinder shaped sample. In this case D is reduces to a minimum value, as will be shown later, and $\chi_{dc} \simeq \chi_0$.

In our measurements we determine the temperature dependence of the susceptibility $\chi_0(T)$. Because our materials are inhomogeneous and complicated, we expect contributions from different origins to our signal. In what fallows we review few known temperature dependent susceptibilities. It should be pointed out that in our measurements at temperatures much higher than T_c of HTSC materials, we observed increasing susceptibility with increasing temperatures, in agreement with previous works [2][3]. The following sections aims at pointing out the conditions in which this could occur.

3.1 Isolated spin susceptibility

According to Langevin paramagnetism equation, the susceptibility of a free spin in the limit $\mu_B H/k_B T \ll 1$ is given by

$$\chi_0 = \frac{N\mu_B^2}{3k_B T} = \frac{C}{T}. \tag{3.1}$$

This result is known as the Curie law and $C \equiv N\mu^2/3k_B$ is the Curie constant, N is number of electron per unit volume. This susceptibility component is expected to be dominant over all other contributions at low temperatures.

3.2 Weakly coupled spins

Weak coupling is when the spins are coupled to each other with weak enough coupling so that the temperature of the experiment could still be considered high compared to the coupling energy. The experimental criteria for weak coupling is that T is much larger than the freezing temperature, which for an antiferromagnet is called T_N. In this case the susceptibility is similar to the one of isolated spins but with a constant added to the temperature, called Curie-Weiss temperature:

$$\chi_0 = \frac{C}{T+\theta}. \tag{3.2}$$

In a ferromagnet θ is negative. In an antiferromagnet θ is positive, namely, the inverse susceptibility above T_N is a linear function of T which crosses the χ_0^{-1} axis at a positive value. Mean field theory based on the Hamiltonian

$$H = \sum_{\langle i,j \rangle} J\vec{S}_i \cdot \vec{S}_j \tag{3.3}$$

Where the sum is over near neighbors localized spins, predicts the expression

$$\theta = \left[\frac{2S(S+1)}{3K_B}\right] \sum_i Z_i J_i \tag{3.4}$$

Where Z is the number of neighbors of a given atom, and J is the exchange integral.

3.3 Pauli spin susceptibility

One might expect that the conduction electrons in metals would give a Curie-type paramagnetic contribution to the susceptibility like for free spins. However, Pauli showed that the application of the Fermi-Dirac distribution gives a different result. The Pauli spin susceptibility of the conduction electron is

$$\chi_0 = \mu_B^2 \mathfrak{D}_{(\epsilon_F)} \tag{3.5}$$

where $\mathfrak{D}_{(\epsilon_F)}$ is the density of state at Fermi energy. This term is independent of temperature. This susceptibility component is expected to dominate at the high range of the temperature, when the contributions from isolated or weakly coupled component will fade out.

3.4 Landau susceptibility

By using Landau macroscopic theory, with the well known Hamiltonian:

$$\hat{H} = \frac{1}{2m}\left(-\imath\hbar\nabla - \frac{q}{c}\vec{A}\right)^2 \tag{3.6}$$

It is possible to conclude the susceptibility of electron's sea in the condition $\hbar\omega \ll k_B T \ll E_F$, when $\hbar\omega = \frac{\hbar e}{mc}B \approx_{B=1T} 10^{-4}_{eV} \sim 1_K$:

$$\chi_L = -2\frac{1}{24\pi^2}\frac{e^2 k_F}{mc^2} \tag{3.7}$$

This diamagnetic contribution is very small, and we neglect it in our experiment.

3.5 Core susceptibility

There are contribution to the susceptibility from the inner electrons of the atoms known as the Van Vleck and Langevin susceptibilities. The Langevin susceptibility emerges from the tendency of electrical charges partially to shield the interior of a body from an applied magnetic field. This contribution is naturally diamagnetic. The Van Vleck susceptibility stems from standard perturbation theory of the wavefunction ground state in a weak field. The Van Vleck susceptibility gives paramagnetic contribution. These contribution are constants as the function of the temperature. They are independent of the Fermi energy of the electrons, but do depend on chemical

composition. It is customary to name these contributions as corr susceptibility and to extract their value from chemical tables.

3.6 Strongly coupled spins susceptibility

It is impossible to exactly solve the susceptibility of Heisenberg spins on a 2D lattice for all temperatures. Yet a lot of insight could be gained from solving just two coupled spins. Consider the Heisenberg model given by the Hamiltonian:

$$H = J\vec{S_1} \cdot \vec{S_2} - \vec{B}(\vec{S_1} + \vec{S_2}) \tag{3.8}$$

in the appendixes we give in detail the exact solution, which leads to:

$$\chi = \lim_{B \to 0} \frac{dM}{dB} = \beta \left[e^{\frac{\beta J}{2}} \cosh\left(\frac{\beta J}{2}\right) \right]^{-2} \tag{3.9}$$

This function is shown in figure 3.1. It is noticeable that for strong coupled spins, there is a region in which χ increases with increasing temperature. It should be added that this conclusion is valid for even more complicated Hamiltonians, such as the 2D Heisenberg model [4], and $t - j$ model that can only be solved numerically.

3.7 Pseudogap

This section contains our interpretation of ARPES measurements in terms of susceptibility [5]. It is well-accepted that the pseudogap have an effect on the density of states at Fermi energy. As discussed earlier this can affect the susceptibility via the Pauli contribution. To account for Pauli χ_0 one simply needs to count states at the Fermi energy for a given value of T/T^* where T^* is the pseudogap temperature. The contribution of states on the Fermi arc are denoted by χ_{arc}, and the left over

states at the pseudogap region are marked by χ_{PG}. The length of the Fermi arc L is proportional to $\frac{T}{T^\star}$. Let's take $A(T)$ to be the height of the ARPES spectral function at the Fermi energy on this arc. This gives

$$\chi_{arc} = A(T)\frac{T}{T^\star}. \tag{3.10}$$

According to the ARPES data, it is hard to express the spectral height as a function of the temperature. We decided that it's reasonable to take $A(T) \approx Constant$, in our approximation. At the part which is pseudo-gaped there is still spectral weight of height smaller also by factor $\frac{T}{T^\star}$ from A. The length of this pseodo-gaped part is proportional to $1 - \frac{T}{T^\star}$. Therefore,

$$\chi_{PG} = A\frac{T}{T^\star}\left(1 - \frac{T}{T^\star}\right). \tag{3.11}$$

Since $\chi = \chi_{arc} + \chi_{PG}$ we expect

$$\chi_0 = A\left(\frac{2T}{T^\star} - \left[\frac{T}{T^\star}\right]^2\right). \tag{3.12}$$

At $T \geq T^\star$, $\chi(T)$ should saturate and become the usual Pauli susceptibility.

We concluded that as a consequence of the pseudogap, the susceptibility should grow as T grows. Since $A(T)$ is not known, any function of T/T^* that grows from zero and saturates at $T/T^* = 1$ could do for interpreting our measurements. As we show later, the function:

$$\chi_{PG} = \frac{Const}{\cosh\left(\frac{T^\star}{T}\right)} \tag{3.13}$$

has the required properties and provide a good fit to the data. In figure 3.1 we show graphically all the above types of susceptibilities: shrinking arcs, strong coupled spins and the pseodogaped fitting function.

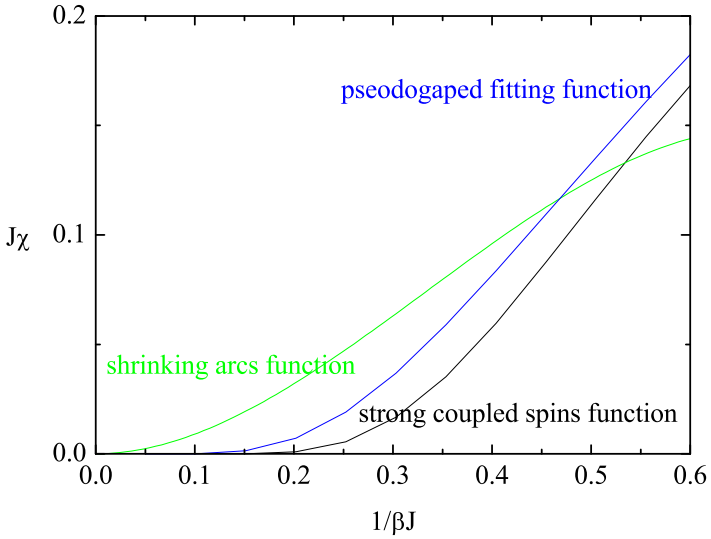

Figure 3.1: The two theoretical function of the "pseodogap's" susceptibility and the fitting one.

Chapter 4

Experimental methods

4.1 The Measurement System

The measurements of this project were taken with the S600 SQUID SUSCEPTOMETER of CRYOGENIC LTD. The SQUID device is shielded by niobium can from environmental magnetic noise and the stray field from the magnet. The pick up coils are wound in a second order gradiometer configuration with only a few millimeters separation between adjacent turns. This configuration is chosen to reject the field from the surrounding magnet to typically 0.1% and hence de-sensitise the SQUID to changes in signal associated with magnet field drift. The SQUID measures relative changes in magnetic flux and for this reason it is necessary to move the sample through the coil set. This causes a screening current to flow in the flux transformer circuit which opposes the resultant change in flux threading the pick up coils. This current is proportional to the induced magnetic moment of the sample and is detected by the SQUID via the input coil. The output from the SQUID electronics then gives a voltage directly proportional to the signal detected at the SQUID sensor.

4.2 The experimental Condition

One of the important parameters in our work is to compare the absolute value of the susceptibility of different samples. For this purpose it was important to keep the same measurement's conditions for all the samples. We used the same sample holder, the same magnetic fields, the same temperature sequence, and the same sample mass (see below) for all the measurements. We repeated each measurement six times in order to increase the signal to noise ratio. Finally, we measured the mass of each sample accurately, and normalized the sample's signal by it.

4.2.1 The sample's mass

Although the signal is normalized by the mass, we tried to use the same mass for all the samples. That's because the mass effects the sample's volume, and the volume effects the magnetization factor. In order to make sure that this factor doesn't effect our mass scale, we measured the normalized signal as a function of the mass. This measurement is presented in figure 4.1, and it is obvious that in samples with mass which is heavier than $m = 0.3_{gr}$, the magnetization factor isn't effective, because the signal is constant. In all our measurement we used $m \simeq 0.8_{gr}$. Measurements with mass bigger than that give roughly the same χ_0. For this mass, the height to diameter ratio of the sample shape is larger than 2, and the sample resembles a needle, where the magnetization factor is zero.

4.2.2 The Magnetic Fields

In order to get a reasonable values of the susceptibility with a reasonable errors, we tried different types of measurements. We scanned a number of fields to decide which

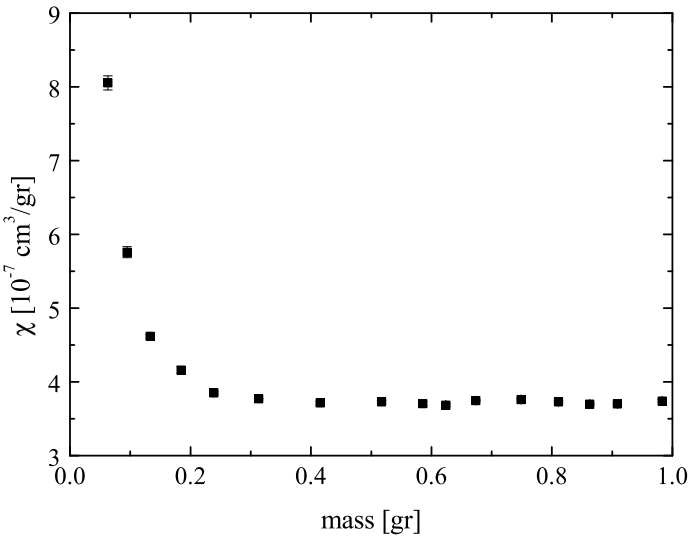

Figure 4.1: The normalized susceptibility as function of mass at T=300K. Our samples masses are in the rage of $m = 0.80(3)$.

fields to use. We found that there is a small difference between the susceptibility at the high and low fields, as shown in figure 4.2. Although it is customery to use the low fields, according to the susceptibility definition, we used the higher fields. That's because in higher fields the magnetic signal is much clearer with much smaller errors, and the magnetic effects that we expect to measure are at the resolution limit of the system in small fields. Moreover, the evolution of the high and low fields measurements is the same for different samples. So, it is fine to compere the susceptibility of different samples, as long as we use the same range of fields for each sample. We examined the influence of taking into account six fields at a small number of temperatures versus taking the measurement at one field but at a large number of temperatures. Of course, in the six fields method the susceptibility's errors were reduced at each temperature, but our ability to extract model parameters was better

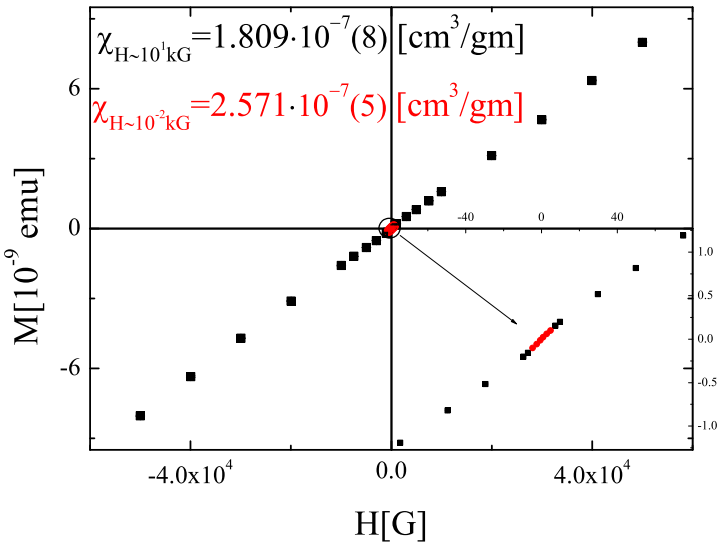

Figure 4.2: The magnetization as function of the field at T=300K. There is a different between the susceptibility at the high and the low fields.

in the one field method. Thus, we set the magnetic field to $H = 9.96kG$, and scanned large number of temperatures, for all the samples.

4.2.3 The measurement's temperature

For each sample, we scan a full range of temperatures from 20K to 310K in steps of 1K. The measurements, for all the samples, were taken with the same sequence. First, cool-down to 20K, and then collecting the data while warming. Of-course, it is important that the temperature will be stable during the SQUID scan, and close to the "set temperature". This is achieved by setting a strict temperature stability condition, $\frac{dT}{dt} \leq 0.0005[\frac{K}{min}]$, and a long waiting time before a measurement starts, 30_{Sec}. Because we used the same sequence for every sample, we got approximately the same temperatures in every scan. Our main interest in this work is the higher

range of the temperatures. e.g, above T_c. Therefore, for the samples with T_c which is higher than 20K, we collected it's data from T_c up.

Chapter 5

Experimental results

In figure 5.1 we present data from four sample of the $x = 0.2$ family with different doping levels. The data contains several features. I) A zoom in on the high temperature region of a single sample, figure 5.2, reveals an increasing of the susceptibility with increasing temperatures. Although in this scale the T dependence at high T seems pretty weak, on a smaller scale it looks much clearer, as will be shown in the next chapter. II) All data sets show a Curie-Weiss type increase of the susceptibility at low temperatures. III) As doping increases the absolute value of the susceptibility at 300K increases.

The first observation is the most important one in this work. The arrows in fig 5.2 mark the minimum of every sample's susceptibility. There is a correlation between this point and the doping level, and as the doping decreases the minimum moves to higher temperatures. This correlation will lead us to a determination of $T^{\star}$ as a function of the doping. The second observation is common to all samples. The CW term could be a result of isolated spins, impurities, or spins on the chain layer. However, it could also be part of a clean 2D layer with conducting coupled

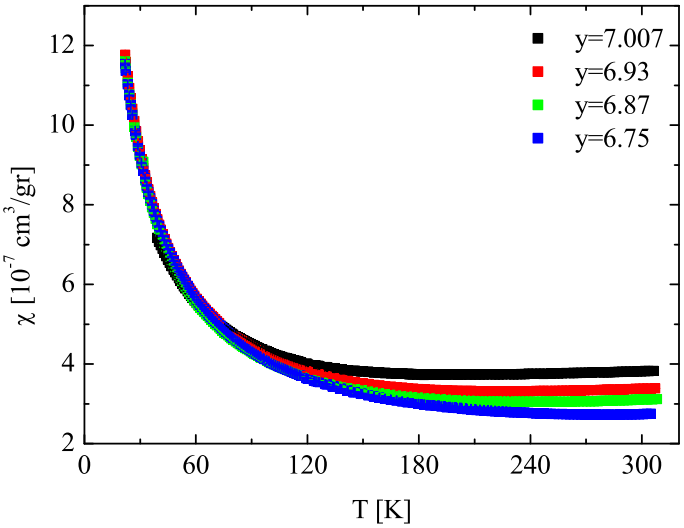

Figure 5.1: Raw data of four samples from the $x = 0.2$ family with a different doping levels.

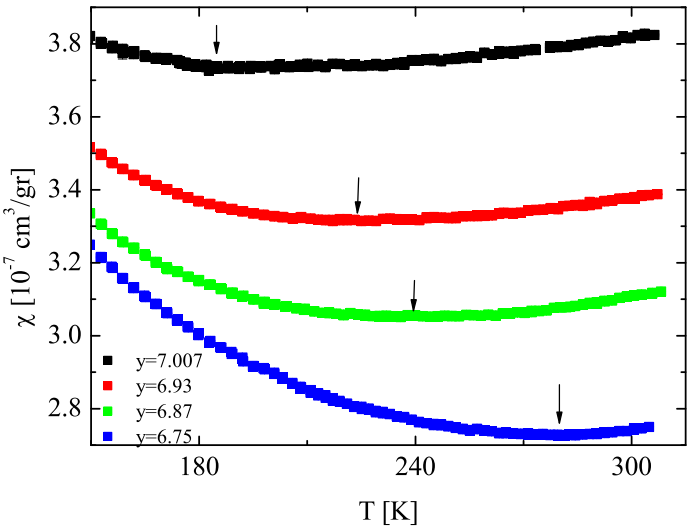

Figure 5.2: Zooming on the raw data of the same four samples. the arrows are pointing on the minimums.

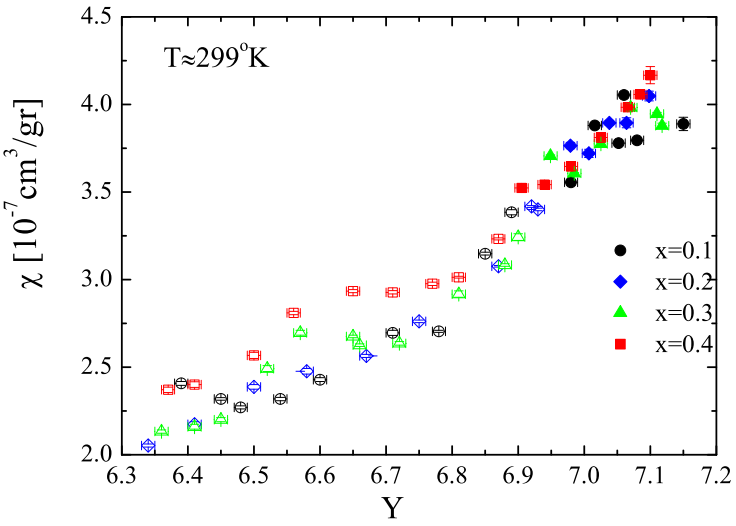

Figure 5.3: The susceptibility of all the samples at $T = 299K$.

electrons susceptibility. The third observation is also universal. In fact, we plot the susceptibility of all the samples at $T = 299$ K in figure 5.3. This data was collected by scanning the magnetization using six different fields, in order to get accurate result at a fixed temperature. The susceptibility on this graph is increasing with doping, probably due to the changes in the fermi level with the doping . These changes affect the pauli susceptibility, as explained before.

Chapter 6

Data analysis

In all cases where a clear minimum in the susceptibility was observed, namely, for supercoducting samples, we fit the data to the three component function

$$\chi_0 = \frac{C_1}{T+\theta} + \frac{C_2}{cosh(\frac{T^\star}{T})} + C_3. \tag{6.1}$$

It is most natural to relate C_1 to the wight of an impurity related CW contribution, C_2 to the pseudo-gaped electrons, and C_3 to free electrons (after cor susceptibility is subtracted). As we explained before, there is no acceptable theory for the pseudogap and no consensus about it's contribution to χ_0. We use the function $C_2 \cosh^{-1}(\frac{T^\star}{T})$ since it roughly behaves as one would expects from the density of states at the Fermi level as determined by ARPES, and because it fits the data very well. It can be perceived in figure 6.1 how well this function fits the data, and how clear the χ minimum is. However, it is possible that the division of χ_0 to impurities, pseudogap,and free electron contribution is artificial, that there are no impurities contribution, and that the susceptibility simply has two energy scales θ and $T^\star$. We will be mostly interested in these two parameters. As for the C's which are determined by the fits, they are found to behave smoothly and monotonically as a function of doping and family as

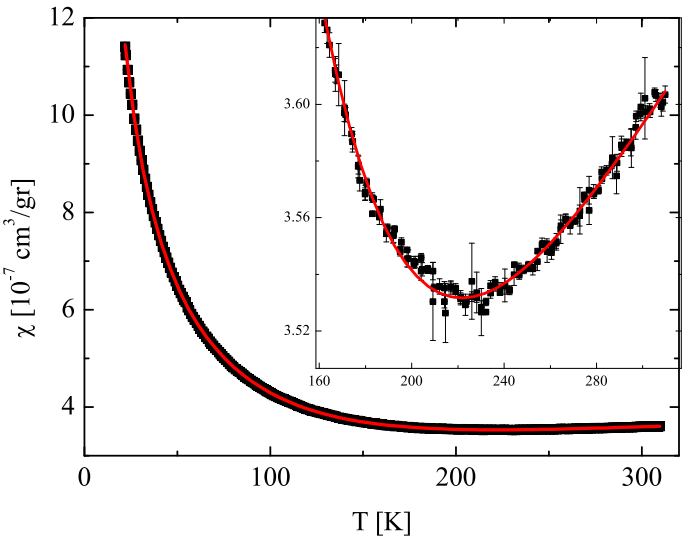

Figure 6.1: The susceptibility raw data and fitting, with a "zoom in" on the region of the increasing susceptibility at high temperatures.

shown in the appendix. It is important to point out that we fitted the data without any restriction, all the parameters are free during the fitting.

Chapter 7

Results and Discussion

As mentioned before we concentrate on the family and doping dependence of $T^\star$ and θ. These parameters are the most reliable result of the fit, because they don't depend on base line shifts or changes in the absolute value of the susceptibility between samples. The result of the other parameter are less relevant to this project, and will be presented in the appendix.

7.1 $T^\star$- The Pseudogap's temperature

This parameter, depicted in figure 7.1, behaves like the well-known $T^\star$ measured by other techniques on a variety of superconductors samples[6] [7]. This lovely result is a strong support of our assumption that the increasing susceptibility with increasing T is related to the Pseudogap physics. For comparison, we depict in fig 7.2 historical results of $T^\star$, for different compounds, and from different techniques [6]. $T^\star$ decreases, approximately linearly, as a function of the doping.

In figure 7.1 we also see the family dependence of the pseudogap. At a first glance

it looks like $T^\star$ has anti-correlation with T_c^{max} or T_N. The $x = 0.4$ family, which has the highest T_c^{max} and T_N, has the lowest $T^\star$. In the other extreme, the $x = 0.1$ family, with its low T_c^{max} and T_N, has the highest $T^\star$. However, this conclusion is reversed if instead of plotting the $T^\star$ as a function of oxygen level, it is properly normalized and plotted as a function of mobile hole concentration ΔP_m. ΔP_m is defined in two steps: I) The chemical doping measured from optimum, $\Delta y = y_0 - y$, is defined for each compound(y_0 is the doping level at which T_c is at maximum). II) In order to make all superconductor domes converge into a single dome, Δy was multiplied by a different constant $K(x)$ for every family leading to the definition $\Delta p_m = K(x)\Delta y$. We used $K(x) = 0.76, 0.67, 0.54, 0.47$ for $x = 0.1, 0.2, 0.3, 0.4$. The constant $K(x)$ represents the fact that not all the chemical holes turns into mobile holes on the $Cu - O$ plans and contributes to the superfluid density.

A previous result of our group was that in a plot of critical temperatures normalized by T_c^{max} vs. Δp_m, not only the T_c curves merge into one, but also the in-plane Heisenberg coupling J_f. This coupling is extracted from T_N by dividing out the contribution from the out-of-plane coupling $J_f\alpha$ [8]. An implication of this scaling is that $T_c^{max} \propto J_f$. We tried the same scaling on the $T^\star$, and plot it in figure 7.3. The scaling is NOT working very well this time. In contrast, if we change the temperature normalization, and instead of using T_c^{max}, we use T_N^{max} (the maximum Nèel temperature), we get a much better scaling (figure 7.4).

This result bares important new information about the $T^\star$. When we normalized the temperature by T_c^{max} we are actually normalizing by J_f. If the pseudogap was a result of magnetic interaction between the spins in the planes (2D model) ONLY, this should have lead to a good scaling. The faliure of the normalization by T_c^{max} suggest that the pseudogap is not a result of 2D magnetic interactions. When we normalized

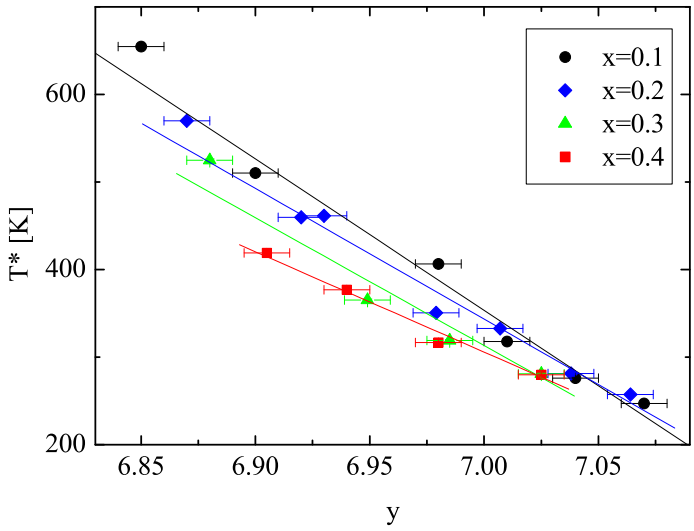

Figure 7.1: The Pseudogap's temperature as a function of doping and families.

the temperature by T_N^{max}, we are taking into the account the coupling between the planes (3D model) as well. The sucsses of the normalization by T_N implies $T^\star$ is governed by 3D magnetic interaction.

7.2 θ-The paramagnetic Curie temperature

Although we didn't expect to find any correlations in this parameter, we got an interesting tendency (see fig7.5) which hints that θ has nothing to do with impurities. In the antiferromagnetic region we found $\theta \sim 0$. As we go to higher doping levels this magnetic energy scale increases. It is also clear that there are variations of θ between the families. The $x = 0.4$ has the strongest θ, and the $x = 0.1$ the weakest. This result is consistent with pervious findings of our group, namely, T_c^{max} is correlated with the magnetic energy scale. In fact, if we plot this parameter as a function of

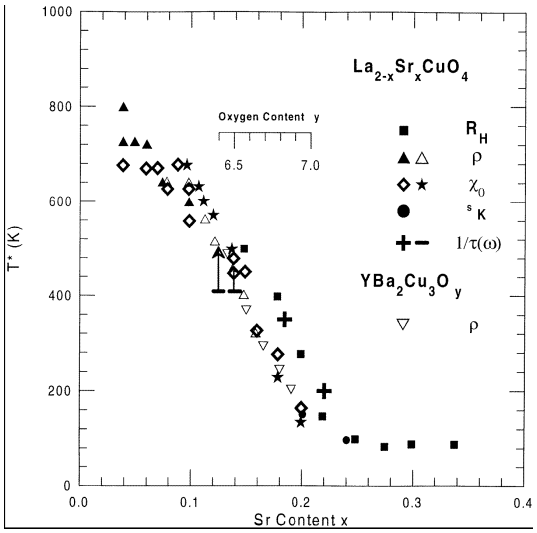

Figure 7.2: Variation of $T^{\star}$ with doping for $La_{2-x}Sr_xCuO_4$ as measured by various probes. The full squares denote the temperature below which the Hall coefficient has a rapid temperature dependence. The open circles refer to maxima in the static susceptibility $\chi_{(T)}$. and the full circles the temperature where the Knight shift starts to decrease. The triangles refer to the temperature where there is a slope change in the dc resistivity, the crosses infrared measurements of $1/\tau$ suppression and the horizontal lines to lower limits of infrared data.

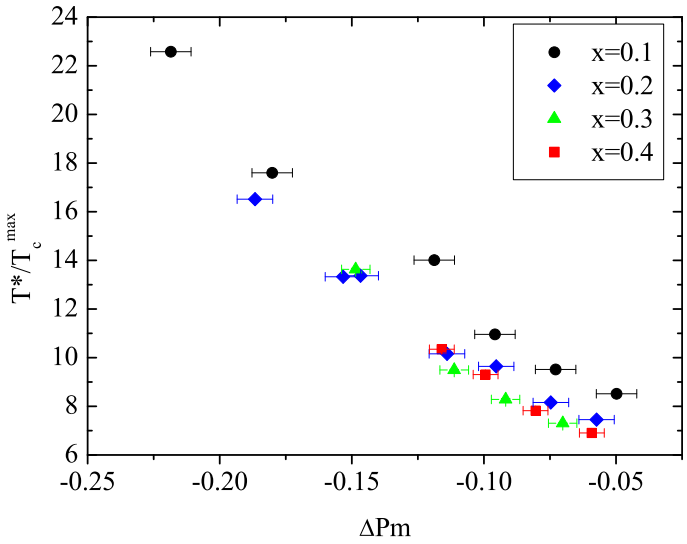

Figure 7.3: The Pseudogap's temperature as a function of hole concentration and families, normalized by T_c^{max}.

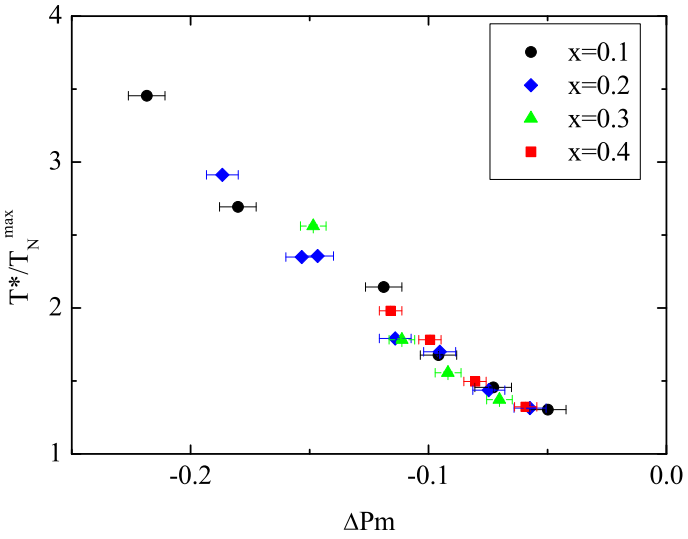

Figure 7.4: The Pseudogap's temperature as a function of hole concentration and families, normalized by T_N^{max}.

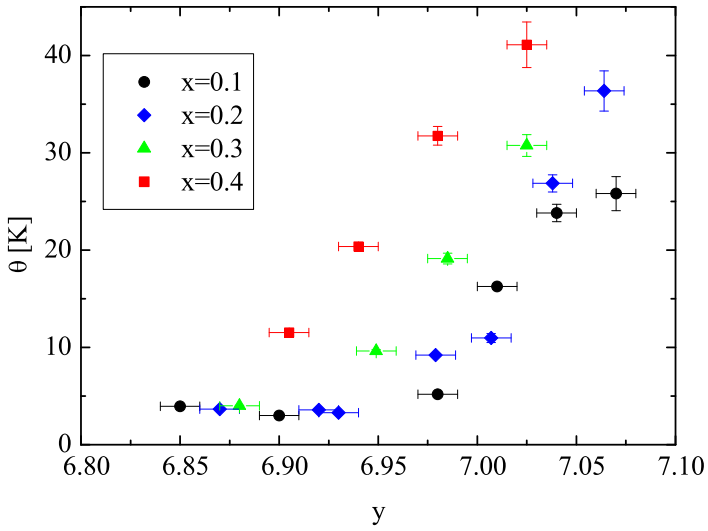

Figure 7.5: The paramagnetic Curie temperature as a function of doping and families.

ΔP_m, we get very nice result as shown on figure 7.6. Once again we find that the proper doping parameter is ΔP_m and not oxygen level y.

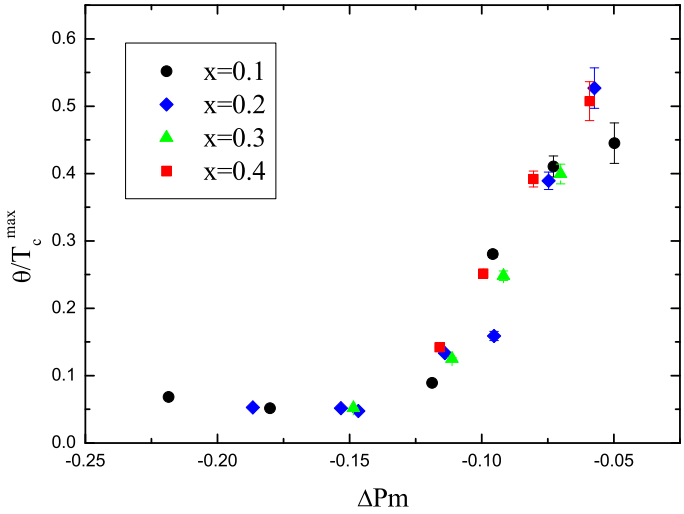

Figure 7.6: The paramagnetic Curie temperature as a function of mobile hole concentration and families.

Chapter 8

Summary

From the susceptibility measurement we succeeded to deduce $T^\star$ of several samples from different families and doping levels. In figure 8.1 we plot the completed phase diagram: T_c, T_N, T_g and $T^\star$.

Although there seems to be an opposite relation between T_c and $T^\star$ by compering it between the families, when we scale the phase diagram to hole mobile concentration, and normalize it by T_N^{max}, we find that all the families merge to one another, as shown in figure 8.2.

The T_c's doesn't merge as well as the other critical temperature. Because the superconducting state is influence by 2D interaction, unlike the other states. Specially the $x = 0.1$ family, that we know from previous results [8], has a much stronger coupling between the planes than the other families. It was suppressing to find that $T^\star$ is influenced by 3D magnetic interaction, and not 2D like T_c.

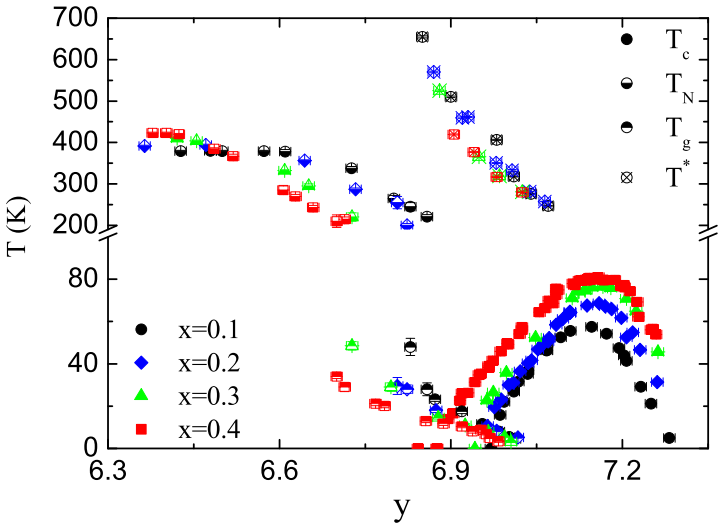

Figure 8.1: The completed phase diagram.

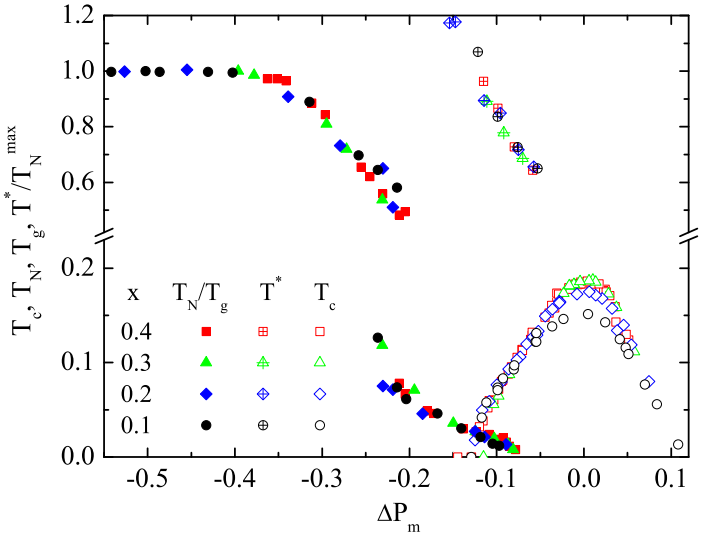

Figure 8.2: The scaled completed phase diagram.

Appendix A

Sample information

A.1 Sample Preparation

CLBLCO samples are prepared by solid state reaction. Raw powders are machine milled and baked in air at $950^o c$ for one day and re-grounded repeatedly 3 times. Then the powder is pressed into pellets, and the pellets are sintered for 70h in flowing oxygen at $960^o c$, and cooled at a rate of $10^o/h$. Different oxygen content is achieved by oxygen reduction in a tube furnace in flowing oxygen at the right temperature. The reduction temperature determines the oxygen doping level in the material. After 48h in the furnace the samples are quenched in liquid N_2. Under a certain doping level (about y=6.7), the reduction is made with flowing nitrogen instead of oxygen (so that more oxygen can come out of the sample at a certain furnace temperature) and quenched to room temperature.

A.2 Samples Characterization

In this project we used 65 different samples. in order to confirm the quality of the samples, we arranged a few test.

A.2.1 X-Ray

Each group of samples, that was made together (there are 8 groups), we scan with X-Ray. According to a storage information about the material, we can confirm the quality of the group. The resolution of the scan can inform us about the family of the group, and about large deviations, if there are such deviations in the samples. in figure A.1, there is one example of the X-Ray scan.

A.2.2 Iodometric Analysis

In this project it is important to know the oxygen content as precise as possible. the X-Ray can't give us that. Redox titrations proved to be the most reliable way to measure the oxidation state of copper and thereby deduce the oxygen content of the CLBLCO. An iodometric method involves two experiments. In Experiment A, $(Ca_xLa_{1-x})(Ba_{1.75-x}La_{0.25-x})Cu_3O_y$ is dissolved in dilute acid, in which Cu^{3+} is converted to Cu^{2+}, and then we can measure the copper quantity .In Experiment B, CLBLCO is dissolved in dilute acid containing I^-. Each mole of Cu^{3+} produces 1 mole of I_3^-, and each mole of Cu^{2+} produces 0.5 mole of I_3^-. And that is enough in order to realize the relation between Cu^{3+} and Cu^{2+} in the sample. This method have a big disadvantage, the double titrations increase the uncertainty. The iodometric procedure give a precision in oxygen content of ± 0.04 in the value of y, which is too high for our work. But in order to calculate the copper's content of the sample, we

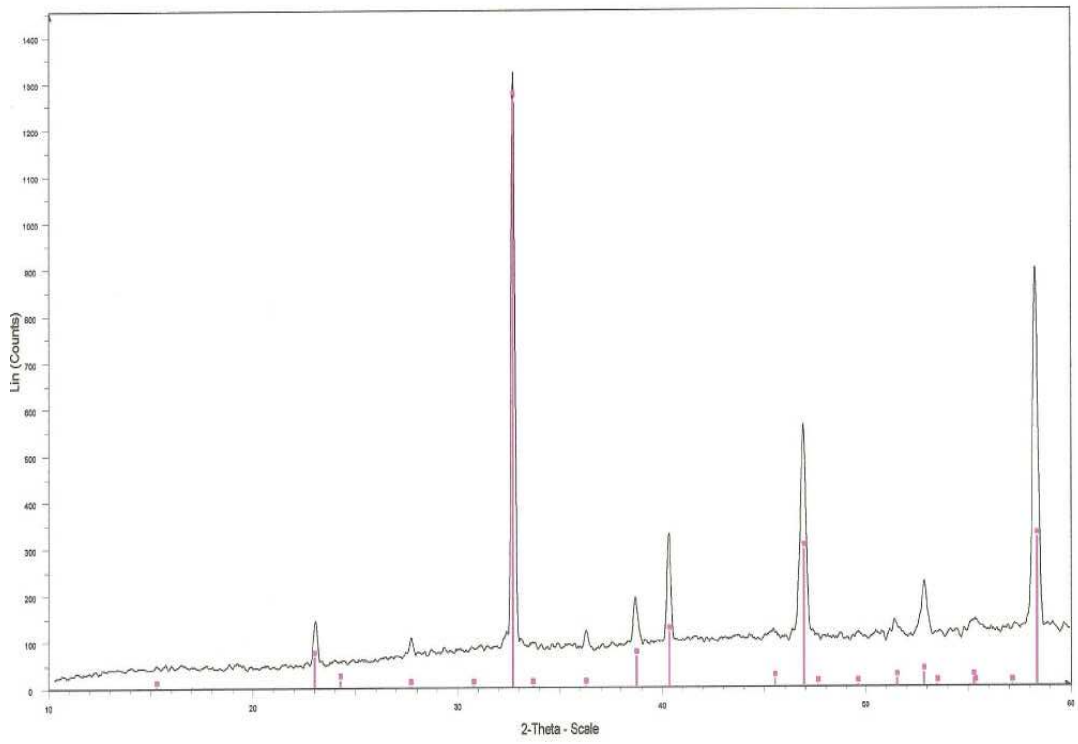

Figure A.1: X-Ray scan of x=0.4 sample.The red picks are the previous information about CLBLCO.

can use Experiment A. This result, together with the X-Ray, gives us control on the sample's quality.

As said, the sample is dissolved in dilute acid, for simplicity, we write the equations for the formula $(Ca_xLa_{1-x})(Ba_{1.75-x}La_{0.25-x})Cu_3O_7$, but you could balance these equations for $y \neq 7$.

$$(Ca_xLa_{1-x})(Ba_{1.75-x}La_{0.25-x})Cu_3O_7+\frac{53}{4}H^+ \longrightarrow \frac{5}{4}La^{3+}+\left(\frac{7}{4}-x\right)Ba^{2+}+xCa^{2+}+3Cu^{2+}+\frac{53}{8}H_2O \tag{A.1}$$

The total copper content is measured by treatment with iodide

$$3C_u^{2+}+\frac{15}{2}I^- \longrightarrow C_uI_{(s)}+\frac{3}{2}I_3^-$$

And titration of the liberated triiodide with standard thiosulfate. Each mole of Cu in CLBLCO is equivalent to 1 mole of $S_2O_3^{2-}$ in the experiment.

A.2.3 Citrate-Complexed Copper Titration

Unlike the traditional iodometric analysis, this procedure directly measures Cu^{3+}. By that, the uncertainty is reduced to $\neq 0.01$, which is sufficient for us. The sample is first dissolved in a closed container with 4.4M HBr, in which $Cu3+$ oxidizes Br^- to Br^{3-}:

$$Cu^{3+}+\frac{11}{2}Br^- \longrightarrow CuBr_4^{2-}+\frac{1}{2}Br_3^- \tag{A.2}$$

The solution is transferred to a vessel containing excess I^-, excess citrate, and enough NH_3 to neutralize most of the acid. Cu^{2+} is complexed by citrate and is not further reduced to $CuI_(s)$.The Br_3 from the reaction oxidizes I^- to I_3^- :

$$Br_3^-+3I^- \longrightarrow 3Br^-+I_3^- \tag{A.3}$$

And the I3 - is titrated with thiosulfate, as seen before. By that we can know the quantity of Cu^{3+} in the sample, and therefor to estimate the oxygen content.

Appendix B

An exact solution to Heisenberg model

As explained on the theoretical background, we said that the exact solution of Heizenberg model of two sites leads to increasing susceptibility as the function of the temperature.

lets us consider Heizenberg model of two spins in two different sites. the hamiltonian:

$$H = J\vec{S_1} \cdot \vec{S_2} - \vec{B}(\vec{S_1} + \vec{S_2}) \tag{B.1}$$

lets start by concentrating on the first term

$$H_1 = J(\vec{S_1} \cdot \vec{S_2}) = J(S_{1x} \cdot S_{2x} + S_{1y} \cdot S_{2y} + S_{1z} \cdot S_{2z}) \tag{B.2}$$

by using the relations:

$$S_+ = S_x + iS_y \tag{B.3}$$

$$S_- = S_x - iS_y \tag{B.4}$$

we get

$$H_1 = J\left[\frac{1}{2}\left(S_{1+}S_{2-} + S_{1-}S_{2+}\right) + S_{1z}S_{2z}\right] \tag{B.5}$$

in this case, there are four states on Hilbert space.

$$|S_{1z}, S_{2z}\rangle = |\uparrow\uparrow\rangle, |\downarrow\downarrow\rangle, |\uparrow\downarrow\rangle, |\downarrow\uparrow\rangle \tag{B.6}$$

now we find the solution of each state by these well-known relations:

$$S_z|j,m\rangle = m|j,m\rangle \tag{B.7}$$

$$S_+|j,m\rangle = \sqrt{j(j+1)-m(m+1)}|j,m+1\rangle \tag{B.8}$$

$$S_-|j,m\rangle = \sqrt{j(j+1)-m(m-1)}|j,m-1\rangle \tag{B.9}$$

$$S_+|\uparrow\rangle = 0 \tag{B.10}$$

$$S_-|\downarrow\rangle = 0 \tag{B.11}$$

and with placing $j = \frac{1}{2}$:

$$H_1|\uparrow\uparrow\rangle = \frac{1}{4}J|\uparrow\uparrow\rangle \tag{B.12}$$

$$H_1|\downarrow\downarrow\rangle = \frac{1}{4}J|\downarrow\downarrow\rangle \tag{B.13}$$

$$H_1|\uparrow\downarrow\rangle = -\frac{1}{4}J|\uparrow\downarrow\rangle + \frac{1}{2}J|\downarrow\uparrow\rangle \tag{B.14}$$

$$H_1|\downarrow\uparrow\rangle = -\frac{1}{4}J|\downarrow\uparrow\rangle + \frac{1}{2}J|\uparrow\downarrow\rangle \tag{B.15}$$

so, in this order of the states we will get the matrix:

$$H_1 = \frac{1}{4}J\begin{pmatrix} 1 & & & \\ & 1 & & \\ & & -1 & 2 \\ & & 2 & -1 \end{pmatrix} \tag{B.16}$$

and after diagonalize

$$H_1 = \begin{pmatrix} \frac{1}{4}J & & & \\ & \frac{1}{4}J & & \\ & & \frac{1}{4}J & \\ & & & -\frac{3}{4}J \end{pmatrix} \tag{B.17}$$

with the eigenvectors

$$|\uparrow\uparrow\rangle, |\downarrow\downarrow\rangle, \frac{1}{\sqrt{2}}\left(|\uparrow\downarrow\rangle + |\downarrow\uparrow\rangle\right), \frac{1}{\sqrt{2}}\left(|\uparrow\downarrow\rangle - |\downarrow\uparrow\rangle\right) \tag{B.18}$$

e.g.

$$(S, S_z) = \begin{cases} (1,1) & E = \frac{1}{4}J \\ (1,-1) & E = \frac{1}{4}J \\ (1,0) & E = \frac{1}{4}J \\ (0,0) & E = -\frac{3}{4}J \end{cases} \tag{B.19}$$

the first three terms are the triplet states, and the last one is the singlet. for $J > 0$, the antiferromagnetism case, the singlet is the ground state.

on the second hamiltonian term, we will define $\vec{B} = B_{\hat{z}}$, so

$$H_2 = -\vec{B}(\vec{S_1} + \vec{S_2}) = -B \cdot S_{z_{total}} = -B(S_{1_z} + S_{2_z}) \tag{B.20}$$

this expression does not change the eigenvectors, because it is clear that $[H_1, H_2] = 0$.

$$H_2 = -B \begin{pmatrix} 1 & & & \\ & -1 & & \\ & & & \\ & & & \end{pmatrix} \tag{B.21}$$

the hamiltonian

$$H = H_1 + H_2 = \begin{pmatrix} \frac{1}{4}J - B & & & & \\ & \frac{1}{4}J + B & & & \\ & & \frac{1}{4}J & & \\ & & & -\frac{3}{4}J & \end{pmatrix} \begin{matrix} (1,1) \\ (1,-1) \\ (1,0) \\ (0,0) \end{matrix} \tag{B.22}$$

the partition function

$$Z = \sum_{\lambda} e^{-\beta E_\lambda} = e^{-\beta\left(\frac{1}{4}J - B\right)} + e^{-\beta\left(\frac{1}{4}J + B\right)} + e^{-\beta\frac{1}{4}J} + e^{\beta\frac{3}{4}J} = 2e^{-\frac{1}{4}\beta J}\left[\cosh(\beta B) + e^{\frac{\beta J}{2}}\cosh\left(\frac{\beta J}{2}\right)\right] \tag{B.23}$$

the eigenvalue of S_z

$$\langle\lambda|S_z|\lambda\rangle = \begin{cases} \langle 1,1|S_z|1,1\rangle = & 1 \\ \langle 1,-1|S_z|1,-1\rangle = & -1 \\ \langle 1,0|S_z|1,0\rangle = & 0 \\ \langle 0,0|S_z|0,0\rangle = & 0 \end{cases} \tag{B.24}$$

and this expression

$$\sum_{\lambda} \langle\lambda|S_z|\lambda\rangle\, e^{-\beta E_\lambda} = 2e^{-\frac{\beta J}{4}}\sinh(\beta B) \tag{B.25}$$

so the magnetization of these two sites is

$$M = \langle S_z\rangle = \frac{\sum_\lambda \langle\lambda|S_z|\lambda\rangle\, e^{-\beta E_\lambda}}{Z} = \frac{\sinh(\beta B)}{\left[\cosh(\beta B) + e^{\frac{\beta J}{2}}\cosh(\frac{\beta J}{2})\right]} \tag{B.26}$$

finally, the susceptibility

$$\chi = \lim_{B\to 0}\frac{dM}{dB} = \beta\left[e^{\frac{\beta J}{2}}\cosh\left(\frac{\beta J}{2}\right)\right]^{-2} \tag{B.27}$$

we plotted this function as the strong coupled spins function in fig 3.1

Appendix C

The fit's parameters

in this work, our main interest is on the temperature energy scale, e.g. $T^{\star}$ and θ. we now present the plots of the other parameters. the C_1 parameter (figure C.1) that can represent the number of free electors per unit cell, C_2 (figure C.2) which indicate about the pseudogap's contribution to the susceptibility, and C_3- the corr susceptibility.

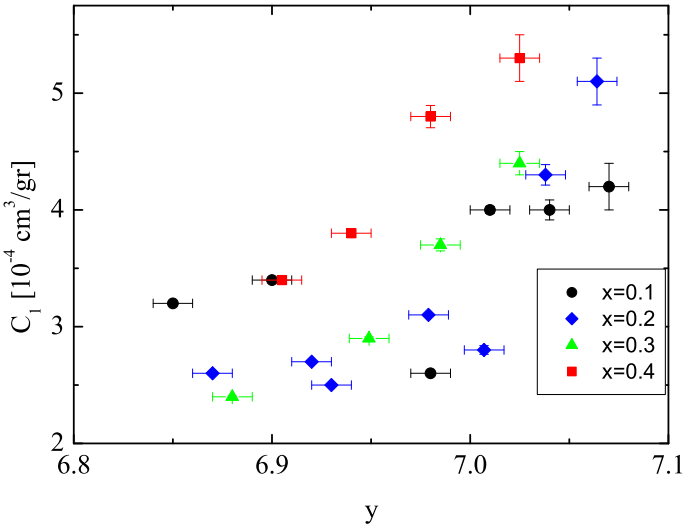

Figure C.1: The parameter C_1 as a function of doping and families

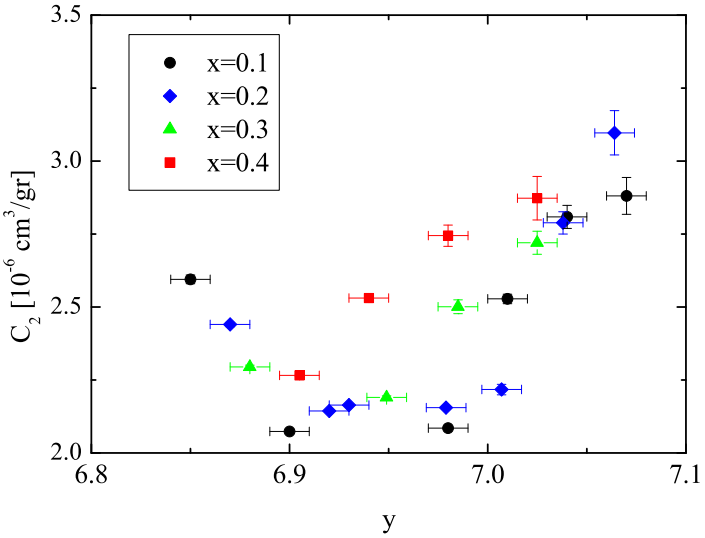

Figure C.2: The parameter C_2 as a function of doping and families

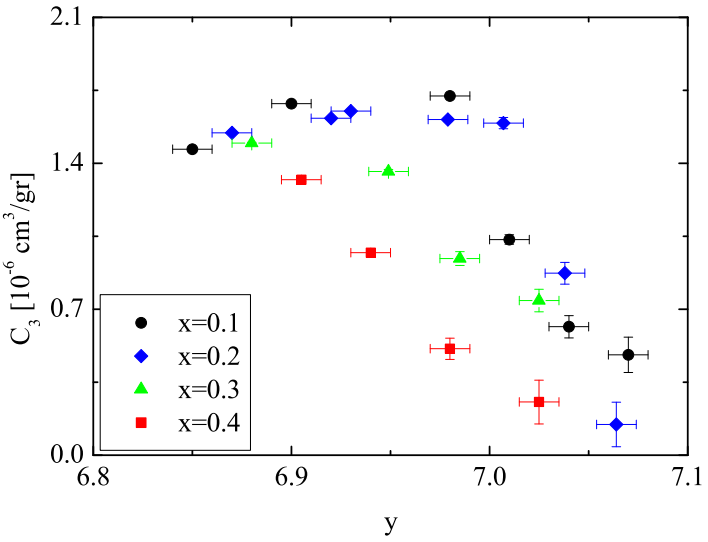

Figure C.3: The parameter C_3 as a function of doping and families

References

[1] O. Chmaissem, Y. Eckstein, and C. G. Kuper, "Structure and a bond-valence-sum study of the 1-2-3 superconductors $(Ca_xLa_{1-x})(Ba_{1.75-x}La_{0.25+x})Cu_3O_y$ and $YBa_2Cu_3O_y$," Phys. Rev. B **63,** 174510 (2001).

[2] D. C. Johnston, "Magnetic Susceptibility Scaling in $La_{2-x}Sr_xCuO_{4-y}$," Phys. Rev. Lett. **62,** 957–960 (1989).

[3] T. Nakano, M. Oda, C. Manabe, N. Momono, Y. Miura, and M. Ido, "Magnetic properties and electronic conduction of superconducting $La_{2-x}Sr_xCuO_4$," Phys. Rev. B **49,** 16000–16008 (1994).

[4] A. Auerbach and D. P. Arovas, "Spin Dynamics in the Square-Lattice Antiferromagnet," Phys. Rev. Lett. **61,** 617–620 (1988).

[5] A. Kanigel *et al.*, "Evolution of the pseudogap from Fermi arcs to the nodal liquid," Nature Physics 2 .

[6] T. Timusk and B. Statt, "The pseudogap in high-temperature superconductors: an experimental survey," Rep. Prog. Phys 62 .

[7] D. K. C. Norman, M. R.; Pines, "The pseudogap: friend or foe of high T_c?," Advances In Physics **54,** 715–733 (2005).

[8] R. Ofer, G. Bazalitsky, A. Kanigel, A. Keren, A. Auerbach, J. S. Lord, and A. Amato, "Magnetic analog of the isotope effect in cuprates," Phys. Rev. B **74,** 220508 (2006).

מקור הפער המדומה בעל מוליכים בטמפרטורות גבוהות

יובל לובשבסקי

מקור הפער המדומה בעל מוליכים בטמפרטורות גבוהות

חיבור על מחקר

לשם מילוי חלקי של הדרישות לקבלת תואר

מגיסטר למדעים

פיזיקה

יובל לובשבסקי

הוגש לסנט הטכניון — מכון טכנולוגי לישראל

ניסן תשס"ז חיפה אפריל 2007

חיבור על מחקר נעשה בהדרכת פרופ. עמית קרן

בפקולטה לפיסיקה

הכרת תודה

אני אסיר תודה לפרופ. עמית קרן על ההדרכה, העזרה והסובלנות.
תודה מיוחדת לרינת עופר על העזרה בתחילת הדרך.
תודה למני שהתקין לי את הלאטך.

אני מודה לטכניון על התמיכה הכספית הנדיבה בהשתלמותי

תקציר

מולכי העל הנחושתיים הם תרכובות קרמיות המכילות מישורים של נחושת וחמצן, הניתנים לסימום על ידי הכנסת חורים טעונים. הכנסת החורים מתבצעת ע"י החלפת אטומים מחוץ למישורים באטומים אחרים בעלי מספר שונה של אלקטרונים ברמה החיצונית. ניתן להסתכל על חומרים אלה כתלות ברמת הסימום: ברמות סימום נמוכות מאוד חומרים אלה הם מבודדים אנטיפרומגנטים. עם עלית רמת הסימום, טמפרטורת המעבר למצב אנטיפרומגנט T_N יורדת מהר מאד, עד שברמת סימום של בערך 4% אין יותר סדר מגנטי לטווח ארוך ועד לאזור שבו מתחילה העל מוליכות ישנו סידור אקראי קפוא של המומנטים המגנטים מתחת לטמפרטורה הקיפאון T_g. זוהי הפאזה הזכוכית הספינית $(spinglass)$, פאזה זו קיימת גם בדגמים על מוליכים בסימום נמוך. עבודות קודמות שנעשו בקבוצה שלנו בדקו את הקשרים בין T_c, T_N ו- T_g. להשוואות כאילו אנו משתמשים במערכת העל מוליכים: $(CLBLCO)$ $(Ca_xLa_{1-x})(Ba_{1.75-x}La_{0.25+x})Cu_3O_y$. מערכת זו יציבה לאורך כל העקומה של T_c. כמו כן היא מאפשרת גמישות רבה בבחירת הדגמים, לדוגמא עבור ערכים שונים של ריכוז ה-Ca ניתן לקבל, על ידי שינוי בריכוז החמצן, קשתות מקבילות של T_c. אופן הכנת הדגמים: תחילה יש לייבש את ה-La_2O_3 במשך שני לילות בטמפ' 1000^o . שבין שני הלילות שוברים מערבבים את החומר, ומחזירים לתנור. לאחר הייבוש מערבבים על-פי יחס המשקלים הרצוי. מערבבים את החומרים היטב. אנו משתמשים ב-$BallMill$. כ-5 דקות במהירות 5, ו-10 דקות במהירות מקסימלית. לאחר ערבוב החומרים מכניסים לתנור: לילה ראשון-900^o , שוברים ומערבבים. לילה שני-920^o , שוברים ומערבבים. לילה

שלישי-945^o , שוברים ומערבבים. בסוף תהליך השריפה משקל הדגם מצטמצם. מכינים פלטי לחץ. כמות החומר ועוצמת הלחיצה נקבעים ע"י התקן הפלט. ומתחילים את תהליך הסינטור, באווירת חמצן: תחילה מחממים ל-960^o למשך 60 שעות, ואז מנמיכים את הטמפ' בצורה מבוקרת ואיטית (כשבוע) עד לטמפרטורת החדר. בסיום תהליך זה קיבלנו דגמים עם חמצון אופטימאלי. ניתן להפחית את רמת החימצון בדגם. כאשר רוצים להפחית במידה ניכרת מבצעים $Reduction$ באווירת חנקן. וכאשר רוצים להפחית בצורה מועטה, מבצעים זאת באוירת חמצן. מניחים את הדגם ברדיד פלאטינום , ומכניסים אותו לתנור $Reduction$, באווירת חמצן. הטמפ' נקבעת על-פי ערך החימצון הרצוי. לסיום התהליך יש לבצע "קוונץ" לחנקן נוזלי, ולהשאיר את הדגם באווירת חנקן עד לייצוב בטמפ' החדר.

תהליך איפיון הדגמים: בעבודה זו חשוב לנו לדעת את כמות החמצן הדגם בדיוק המירבי. בעל-מוליכים ניתן להשתמש בטיטרציה יודומטרית על-מנת למצוא את כמות החמצן בחומר. ב-$CLBLCO$ זה הפרמטר y על פי הנוסחה הכימית. פרמטר זה חשוב באפיון הדגם ומשפיע רבות על תכנותיו כעל מוליך. ידוע כי בפאזה העל-מוליכה של החומר חלק מהנחושת ב-$CLBLCO$ היא במצב הלא שכיח,Cu^{+3}. לפי כמות ה-Cu^{+3} ניתן להסיק את ערכו של ה-y. המצבים השכיחים של הקאלציום, לאנטנום והבריום הם Ca^{+2}, La^{+3} ו-Ba^{+2} , ושל נחושת הם Cu^{+2} ו- Cu^{+3}. במידה וכל הנחושת היתה במצב Cu^{+2}, אז על פי איזון הנוסחה הכימית הינו מקבלים ש- $y = 6.625$, עם מטען קטיוני של $+13.25$ ומטען אניוני של -13.25. במידה וקיים בחומר המצב Cu^{+}, כמות החמצן תהיה עוד יותר קטנה מ-6.625 בנוסחת תא היחידה, ואז ברור כי אנו רק מתרחקים מהפאזה העל-מוליכה. ז"א שהרכב החומר מצריך קיום Cu^{+3} הנדיר יחסית. אם-כן, על פי יחס ה-Cu^{+3} מכמות הנחושת הכוללת בחומר ניתן להסיק את ערך ה-y. אחת השיטות הנפוצות לביצוע המדידה היא בדיוק ביצוע מדידות אילו- תחילה ממירים את כל ה-Cu^{+2} ל-Cu^{+3} , ומודדים את כמות הנחושת הכוללת בחומר. ולאחר מכן מבצעים טיטרציה נוספת אשר בה מודדים רק את ה-Cu^{+3}. ובסופו של דבר, משני נתונים אילו ניתן להסיק את כמות החמצן בתא היחידה. שיטה נחמדה ויעילה אחרת היא $Citrate - ComplexedCopperTitration$.

בשיטה זו מודדים ישירות את ה-Cu^{+3} , ומנתון זה מסיקים את ה-y. לשיטה זו יש יתרון בולט, מלבד הנוחות של ביצוע טיטרציה אחת במקום שתיים, טווח שגיאה שלה נמוך יותר משמעותית. לעומת זאת, לשיטה הראשונה יש גם כן יתרון בכך שמבצעים מדידה לכמות הנחושת הכוללת, מדידה זו יכולה לשמש כבדיקת איכות הדגם, וע"י כך ניתן לראות אם הדגם הורכב כהלכה. במידה ואחוז הנחושת בחומר אינו תואם את האחוז בנוסחת תא היחידה, יש להסיק כי הדגם פגום. מן- הסתם, כאשר הדגם פגום (אחוז גבוה או נמוך מידי של נחושת), כמות החמצן בדגם לא תהיה כמצופה. לכן בד"כ רצוי לבצע רק את שיטת הטיטרציה השנייה, ורק אם תוצאת הטיטרציה אינה הולמת את המצופה, מבצעים את השיטה הראשונה והמסורבלת יותר. תיאור מפורט של שיטות אילו מופיע בנספח העבודה.

כל x שונה מהווה משפחה שונה של על מוליכים בעלת צימוד מגנטי שונה. עבודות אלה הדגימו שבעל מוליכים הנחושתים מתקיים הקשר:

$$T_c \propto J_f n_s$$

כאשר J_f הוא קבוע של הייזנברג (לאינטראקציה מגנטית) עבור משפחה של על מוליכים ו-n_s היא צפיפות נושאי המטען העל מוליך. בקבוצה שלנו נמצא אישור ניסיוני ברור לכך ש J_f הוא קבוע למשפחה נתונה ולכך שיש קורלציה בין T_c^{max} טמפרטורת המעבר לעל מוליך ברמת סימום אופטימלית, לבין T_N טמפרטורת המעבר לאנטיפרומגנט. על פי דיאגרמת הפאזות של ה-$CLBLCO$ ניתן לראות כי המשפחה בעלת טמפרטורת מעבר לעל מוליך בסימום אופטימלי T_c^{max} גדולה יותר, ולכן גם J_f גדול יותר, היא גם המשפחה בעלת טמ- פרטורת מעבר לאנטיפרומגנט T_N גדולה יותר. מתוצאות אילו הנחנו כי הסיבה להבדל בT_c^{max} בין המשפחות השונות של $CLBLCO$ נובע מההבדל בJ_f בין המשפחות ולא מה- הבדל במספר נושאי המטען בסימום אופטימלי.

בפרוייקט זה מדדנו סוספטיביליות בעזרת מגנומטר $SQUID$. מגנומטר זה מורכב

מהתקן על מוליך המכיל שני צמתי ג'וזפסון המחוברים במקביל. התקן זה מאפשר למדוד שינויים בשדות מגנטיים ברזולוציה רגישה ביותר. במגנומטר זה אנו יכולים לשלוט בגודל השדה המגנטי החיצוני, ובטמפרטורת המדידה. ביצענו את כל המדידות שלנו בשדה בעצמת אחד טסלה, וסרקנו את תחום הטמפרטורות מעשרים מעלות קלווין ועד טמפרטורת החדר. הקפדנו לשמור על תנאים דומים ככל האפשר בכל המדידות, ולכל הדגמים השונים.

בעבודה זו הצלחנו להסיק את טמפרטורת המעבר מהפאזה "הנורמלית" ל"פסאודוגאפ" ($Pseudogap$). בניגוד למוליכי על "רגילים" אשר בהם נפתח פער האנרגיה בסמוך לטמפרטורה הקריטית לעל מוליכות, T_c, בעל מוליכים בטמפרטורות גבוהות נמצא שמתחיל להיפתח פער אנרגיה כבר בטמפרטורות גבוהות יותר. בדגמים בעלי רמת סימום נמוכה טמפרטורה זו היא הגבוהה ביותר, ועם עליית הסימום טמפרטורה זו יורדת, בקירוב לינ-יארי, עד לערכה המינימאלי בסמוך לסימום האופטימאלי. טמפרטורה זו מכונה T^*. מכיוון שמעבר פאזות זה אינו חד וברור, קשה להבחין ולהגדיר בדיוק מירבי את ערך טמפרטורה זו. במדידות הסוספטיביליות מצאנו כי בטמפרטורות גבוהות הסוספטיביליות עולה, בניגוד לתוצאה המצופה שהסוספטיביליות תישאר קבועה. כאשר אנו נמצאים בטמפרטורות נמוכות , הספינים החופשיים גורמים לעליית הסוספטיביליות ע"פ עקרונות קירי וייס. ובטמפרטורות הגבוהות אנו מצפים לסוספטיביליות קבועה, ע"פ סוספטיביות לנדאו ופאולי. אנו מניחים שתופעה זו קשורה לפסאודוגאפ. ניתן להבחין שנקודת המינימום של הסוספטיביליות ושיפוע העליה אחריה, משתנים כפונקצית הסימום של הדגם. הגדרנו את טמפרטורת המעבר בעזרת פונקצית מגמה (fit) המתאימה ביותר לנתוני תוצאות המדידה. בפונקציה זו ישנם שלושה איברים: איבר קירי-וייס, איבר קבוע ואיבר פסאודוגאפ. איבר הפסאודוגאפ מורכב מפונקציה היפרבולית, בעיקר עקב ההתאמה המצויינת שלה לנתוני הניסוי. מכיוון שאין עדיין תיאוריה מבוססת לפער המדומה, אין עדיין פונקציה מסכמת להתנהגות הסוספטביליות כתלות בטמפרטורה. ואכן קבלנו מדרך זו את ההתנהגות הידועה של T^* כפונקציית הסימום. בצענו מדידות אילו לכל המשפחות וכך

הגענו לדיאגרמת הפאות הכוללת של המערכת. כאשר ניסינו למצאו קורלציה בין $T^\star$ ל- T_c גילינו שההתאמה בין המשפחות לטמפרטורות קריטיות אלו אינו מושלם. אך כאשר בדקנו את הקורלציה בין $T^\star$ ל- T_N מצאנו התאמה טובה מאד.

המסקנה מגילוי זה הוא שמקור הפער המדומה נובע מאינטרקציות מגנטיות תלת מימ-דיות כמו ב-T_N, זאת אומרת שגם הצימוד המגנטי בין המישורים משפיע על הפער ולכן גם על ה-$T^\star$. זאת לעומת בפאזה העל מוליכת שמושפעת רק מאיטרקציות דו מימדיות, הכוחות המגנטיים בתוך המישורים. תוצאות עבודה זו גם מחזקות את המסקנות הקודמות של קבוצת המחקר שלנו בנוגע לחשיבות האינטרקציות המגנטיות במנגנון העל מוליכות בטמפרטורות גבוהות.